

# Corrections for the Effects of a Radome on Antenna Surface Measurements Made by Microwave Holography

Alan E. E. Rogers, *Member, IEEE*, Richard Barvainis, P. J. Charpentier, and Brian E. Corey

**Abstract**—Measurements of the surface deviations of a parabolic antenna by microwave holography have been corrected for the effects of an enclosing radome. The largest correction, which is due to diffraction from the metal space frame, is made by using a model computed from the radome structure. This model accounts for the changing diffraction as the antenna is scanned during the interferometric mapping of the complex beam pattern. Correction for reflections from the radome panels is made by simultaneously measuring the beam pattern at multiple frequencies to provide delay discrimination to reject antenna side lobes generated by multiple reflections which arrive with delays different from that of the main beam.

## I. INTRODUCTION

THE technique of measuring the complex beam pattern and taking the two-dimensional Fourier transform to obtain the surface deviations has become widely used for surveying large parabolic antennas. The method, known as microwave holography, was first described by Scott and Ryle [1] and is based on the holographic method of Bennett *et al.* [2]. We have used this method to measure the figure of the surface of the Haystack 37 m antenna [3]. The measurements use geostationary satellite transmissions in the 12 GHz band as a signal source. The surface measurements are needed as input to a mechanical model of the antenna used to make adjustments to the surface for operation at wavelengths as short as 3 mm (100 GHz). As the resolution of the holographic measurements was improved to meet the demands of the mechanical model, various corrections were needed to remove errors in the holographic surface maps. Apart from the blockage of the surface by the radome structure, the major contributor to error was found to be reflections from the radome panels. Blockage by the subreflector and its supports also produces large errors but only in very localized regions. We have found it possible to make corrections to reduce the root mean square (rms) error [4] in the surface measurement to less than 0.12 mm with 50 cm resolution. Lower resolution holographic maps have even less error. The use of a shorter wavelength for holography would reduce the errors still further. Unfortunately we were unable to find a suitable signal source at a shorter wavelength which was

continuously available at a constant elevation in the range 30° to 50°.

## II. DIFFRACTION BY RADOME SPACE FRAME

### A. Fresnel Diffraction Integral

The Haystack antenna is enclosed in a geodesic dome with an aluminum space frame [5] of 456 hubs and 1385 interconnecting spars. The Fresnel diffraction pattern for a satellite signal can be computed from the normalized Fresnel integral [6]

$$D(x, y, a, b) = \left[ \frac{i}{\lambda d} \right] \int e^{-i\pi s^2 / (\lambda d)} dA, \quad (1)$$

where

- $x, y$  = rectangular coordinates in aperture plane (see Fig. 1)
- $a$  = antenna azimuth relative to satellite
- $b$  = antenna elevation relative to satellite
- $d$  = distance of obscuring element from reflector surface
- $s$  = perpendicular distance of an element of the wave front passing through the radome from the direct ray between the radio source and the point  $(x, y)$  on the reflector surface
- $dA$  = element of surface area
- $\lambda$  = wavelength ( $\approx 2.5$  cm for 12 GHz band)

Fig. 1 illustrates the geometry used for calculation of the diffraction. An element of blockage is shown at a distance  $s$  from the direct ray and a distance  $d$  from the surface.

### B. Effect on Beam Pattern

The beam response for an aperture illuminated with the diffraction wave front is

$$B(a, b) = \iint_{\text{over aperture}} D(x, y, a, b) e^{ikF(x, y, a, b)} dx dy, \quad (2)$$

where  $k$  is the wave number  $2\pi/\lambda$  and  $F$  is the phase advance of a ray at  $(x, y)$  for scan angles  $(a, b)$ .

For an antenna with intersecting rotation axes,  $F$  may be expressed as

$$F = x \sin a \cos \theta + y (\cos \epsilon \sin \theta - \sin \epsilon \cos \theta \cos a) + z (\sin \epsilon \sin \theta + \cos \epsilon \cos \theta \cos a - 1), \quad (3)$$

Manuscript received April 1, 1992; revised August 28, 1992. This work was supported by the National Science Foundation, Division of Astronomical Sciences.

The authors are with the Haystack Observatory, Massachusetts Institute of Technology, Westford, MA 01886.  
IEEE Log Number 9205494.

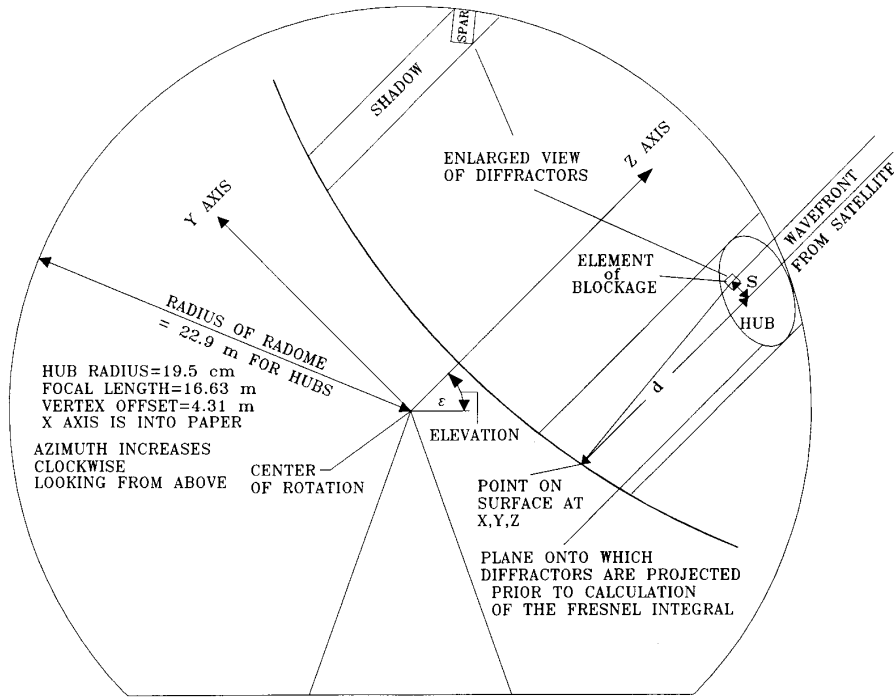


Fig. 1. Simplified antenna and radome geometry.

where  $\theta$  is the satellite elevation (assumed fixed during holographic map) and  $\epsilon$  is the antenna elevation ( $\epsilon = \theta + b$ ). The parameter  $z$  is the perpendicular distance from the aperture plane through  $(x, y)$  on the surface of the reflector to the intersection of antenna rotation axes. The  $xyz$  coordinate system is centered on the intersection of axes with the  $z$  direction along the parabolic axis as shown in Fig. 1. From the geometry of the parabolic reflector the distance  $z$  is given by

$$z = h + (x^2 + y^2)/(4f), \quad (4)$$

where  $h$  is the distance from the vertex to the axis intersection (4.31 m for Haystack) and  $f$  is the focal length (14.6 m for Haystack).

For small scan angles expression (3) becomes

$$F = xa \cos \theta - y(b - (a^2/2) \sin \theta \cos \theta) - z((a^2/2) \cos^2 \theta + b^2/2). \quad (5)$$

Expression (5) and all succeeding expressions are expanded to include only the linear and quadratic terms in the scan angles. Higher order terms in  $a$  and  $b$  are omitted.

### C. Smearing of Diffraction Pattern with Antenna Motion

The diffraction pattern moves on the surface of the reflector as the antenna is scanned because the radome is fixed. The motion  $\Delta x$ ,  $\Delta y$  relative to the antenna coordinate frame  $(x, y, z)$  is given by

$$\Delta x = za \cos \theta - ya \sin \theta \quad (6)$$

$$\Delta y = -zb + xa \sin \theta. \quad (7)$$

For small values of  $\Delta x$  and  $\Delta y$ , this motion changes the phase of the diffracted wave front so that

$$D(x, y, a, b) \simeq D(x, y) e^{ikG(x, y, a, b)}, \quad (8)$$

where

$$D(x, y) = D(x, y, 0, 0)$$

and

$$\begin{aligned} G &= \Delta xa \cos \theta - \Delta yb \\ &= -xab \sin \theta - ya^2 \sin \theta \cos \theta \\ &\quad + z(a^2 \cos^2 \theta + b^2). \end{aligned} \quad (9)$$

The variation of  $d$  in (1) with the scan angles is small enough to produce no significant error in the approximation (8). The approximation will, however, be inaccurate for the extreme outer radius near the edge of the dish where the diffraction pattern moves on and off the surface as the antenna is scanned.

To obtain a map of the antenna surface  $A(x, y)$  the beam pattern is Fourier transformed so that

$$A(x, y) = \iint_{\text{over beam pattern}} B(a, b) e^{-ikH(x, y, a, b)} da db \quad (10)$$

where

$$\begin{aligned} H &= xa \cos \theta - y(b - (a^2/2) \sin \theta \cos \theta) \\ &\quad - z_0((a^2/2) \cos^2 \theta + b^2/2) \end{aligned} \quad (11)$$

and  $z_0$  is the average value of  $z$ . This  $z$  dependent phase correction term is described by Scott and Ryle [1] and is applied before Fourier inversion. A sharper map could be made

using a transform for which  $H = F$  but this would preclude the use of the fast Fourier transform (FFT) algorithm. The loss of resolution which results from assuming a constant value of  $z$  is small for the scan widths used in the mapping. The value of  $z_0$  used in the mapping is, however, needed to calculate an accurate model for correction of the radome diffraction.

#### D. Radome Diffraction Model

The radome diffraction model  $R(x, y)$  corrected for the smearing and resolution of the holography is obtained by substitution of expression (8) into the transform (2) and applying the reverse transform (10) so that

$$R(x, y) = \int \int \int \int D(x', y') e^{ik(F+G-H)} da db dx' dy' \quad (12)$$

$$= \int \int_{\text{over aperture}} D(x', y') \left[ \int \int_{\text{over scan}} e^{ik(F+G-H)} da db \right] dx' dy' \quad (13)$$

where

$$\begin{aligned} F + G - H &= (x' - x)a \cos \theta - (y' - y)b \\ &+ \left( (a^2/2) \cos^2 \theta + b^2/2 \right) (z + z_0) \\ &- ya^2 \sin \theta \cos \theta - xab \sin \theta. \end{aligned} \quad (14)$$

An equivalent expression for (12) and (13) is given by the convolution of the diffraction with the resolution or smearing function  $W$ :

$$R = D \otimes W. \quad (15)$$

The resolution function  $W$  is complex and is a function of the scan width as well as of the location on the antenna. For a discrete scan,

$$W(x' - x, y' - y, x, y) = \sum_{\text{over points scanned}} e^{ik(F+G-H)}. \quad (16)$$

For the radome diffraction model to be accurate, it is important that the same raster scan be used for the radome model as for the holographic map. For high-quality holographic maps a square region was scanned but only a circular portion (or window) was used in order to minimize the resolution side lobes. The complex radome correction  $R(x, y)$  is normalized so that it has unit magnitude and zero phase without diffractors. The complex holographic map whose magnitude represents the surface illumination and whose phase represents small surface deviations is corrected by dividing the map by  $R(x, y)$ .

#### E. Computing the Diffraction Integral and Smearing Function

To ease the computing burden, the Fresnel diffraction integral is computed by summing over the regions of geometrical obscuration rather than the larger clear areas. The Fresnel sum is then obtained from the following relation:

$$\sum_{\text{clear areas}} = \sum_{\text{all areas}} - \sum_{\text{blockage}} \quad (17)$$

$$= 1 - \sum_{\text{blockage}}. \quad (18)$$

This is equivalent to calculating the forward scattering [7] with induced field ratio (IFR) equal to  $-1$ .

Since the smearing of the radome, owing to the resolution and motion of the diffraction pattern, changes gradually with location on the antenna, the smearing function  $W$  is computed for relatively large ( $6 \text{ m} \times 6 \text{ m}$ ) regions.

The computation of a radome correction for a holographic map of 0.5 m resolution takes about 4 h on a computer that executes about 2 million floating point operations per second. Since the geostationary satellites move very little it was generally necessary to compute only one model for a given resolution on each satellite.

#### F. Parameters in Computation

Prior to convolution, to account for the change of diffraction with scanning, the diffraction  $D(x, y)$  is computed for a fine grid of points on the antenna surface. For each surface grid point  $(x, y)$  the diffraction is computed by first projecting the radome hubs and spars onto a plane "diffraction" grid normal to the direction of the satellite, and then summing the points on this diffraction grid to approximate the integral of (1). The center of this diffraction grid is the intersection of the line of sight to the satellite with the radome as illustrated in Fig. 1. The Fresnel integral for an adjacent point on the surface is computed by summing points in the same diffraction grid with suitable translation of its origin. A new diffraction grid is computed once the surface point lies outside a cell whose size is defined by the spacing needed for the correction model. The diffraction grids form a mosaic of the blockage, each grid being adequate for the diffraction computation of a small region and having an extent large enough to include only those diffractors which are close enough (within a few Fresnel zones) to be significant. A more complete geometry of the Haystack antenna is shown in Fig. 2. The space frame geometry is computed from a table of the hub coordinates and a list of the interconnecting spars. Since the Haystack radome structure repeats every  $72^\circ$  in azimuth, the coordinates for only one-fifth of them are needed. While the space frame geometry is thought to be accurate to 1 cm, tests were made to check the registration of the radome with the antenna surface. In these tests a shift in registration of about 10 cm was needed to produce a significant change in the radome diffraction model.

Many tests were made to determine grid spacing required for sufficient accuracy to reduce errors in the model below 10% without adding an excessive computing burden. These parameters are given in Table I.

#### G. Corrections for Satellite Polarization

Small corrections [8] for the linear polarization of the satellite are made to the integral (1) to account for the polarization-dependent IFR of the spars. Spars parallel to the incident electric field vector have a cross-section enhancement of about 20% and about  $10^\circ$  added phase delay. The IFR corrections decrease toward the edge of the aperture as the projected blockage increases owing to the orientation of the spars, which have a  $8 \text{ cm} \times 13 \text{ cm}$  ( $\approx 3\lambda \times 5\lambda$ ) rectangular cross section.

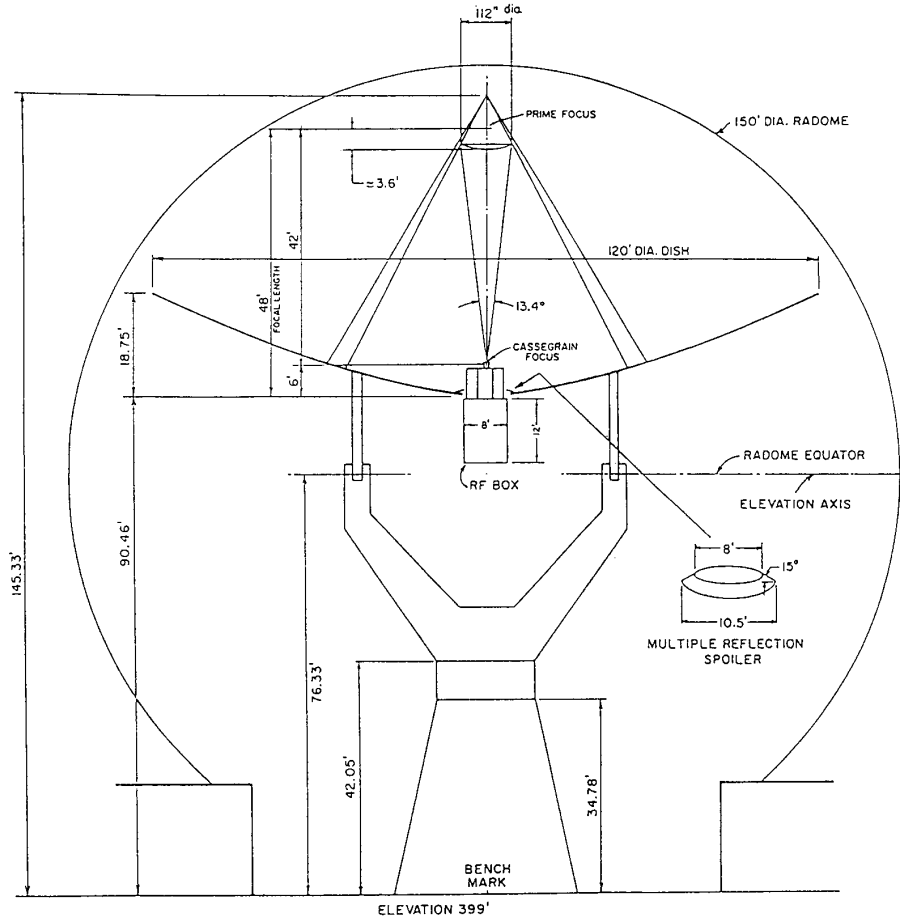


Fig. 2. Dimensions of the Haystack antenna and radome in feet (30.48 cm) and inches (2.54 cm).

TABLE I  
PARAMETERS USED IN DIFFRACTION CALCULATIONS

Parameter	Value
Diffraction grid spacing	3.8 cm
Extent of each diffraction grid (full width)	1.8 m
Surface grid spacing for diffraction prior to convolution	2.0 cm
Surface grid spacing for model output after convolution	17.7 cm
Array size for model output	256 × 256
Grid spacing for change of smearing function	6.1 m

### III. RADOME PANEL REFLECTIONS

The surface maps are also significantly corrupted by reflections from the radome panels. These reflections are best viewed in the transmit mode. Portions of the emerging wave front are backscattered from the panels and retransmitted. These reflections produce side lobes of approximately  $-50$  dB (at 12 GHz) that corrupt high-resolution maps by producing significant corruption of the beam maps at angles of more than  $1^\circ$  from the central beam. It is not possible to model these

reflections, as their amplitude and phase cannot be accurately predicted. In fact, the phase and amplitude of the Haystack antenna side lobes change with the motion of the panels as the radome is pressurized to prevent buffeting of the panels in the wind. The practical solution is to provide some delay discrimination to reject the reflections that have an added signal delay equal to twice the distance from the surface to the panel. Most of the side lobes within a few degrees from the main beam are produced by panels close to the subreflector so that a frequency difference of about 4 MHz will result in a  $180^\circ$  phase shift of the unwanted reflection. Fortunately we were able to find satellites with two bands of pseudo-noise separated by approximately 4 MHz, thereby allowing beam maps to be obtained simultaneously at the two frequencies. When the beam maps are added, the panel reflections largely cancel.

### IV. OTHER CORRECTIONS

#### A. Multiple Reflections from the Subreflector

Artifacts were also produced by multiple reflections on the antenna. The worst multiple reflections for Haystack

are between the subreflector and the region blocked by the subreflector. The blocked or shadowed region includes the feed itself, the front of the RF box (see Fig. 2), and an annulus of the main reflector. The first step taken to eliminate these artifacts, which have the appearance of Newton's rings (see Fig. 7), was to cover the front of the RF box with microwave absorber and to construct a "spoiler" (shown in Fig. 2) to redirect the reflections from the blocked annulus on the main reflector away from the subreflector. The second step was to sum two surface maps taken with subreflector axial positions differing by  $\lambda/4$ . Since the  $\lambda/4$  change in focus is quite small, the major difference in the maps is an approximately  $180^\circ$  change in the phase of the unwanted reflections so that the artifacts are almost canceled in the sum. However, sufficient rejection of the Newton ring artifacts was obtained by a combination of the spoiler and the two-frequency method used to reject the artifacts arising from the reflections from the radome panels. The radome panel reflection delay is about  $0.12 \mu\text{s}$  (thereby repeating about every 8 MHz) while the multiple reflection from the subreflector is about  $0.09 \mu\text{s}$  so that both are significantly reduced by two frequency bands 4 MHz apart. If the satellite transmissions contained pseudo-noise bands spread over a wide band, it would be possible to use the very long baseline interferometry (VLBI) [9] bandwidth synthesis technique or a single wideband channel to provide sufficient delay resolution to eliminate all multiple reflections with delays greater than the inverse bandwidth.

### B. Subreflector Diffraction

The subreflector diffraction produces a significant error in the surface maps towards the edge of the dish. The diffraction is computed using the method of physical optics described by Rusch and Potter [10] and Kouyoumjian [11]. The diffraction pattern is now fixed to the antenna so that  $\Delta x$  and  $\Delta y$  in (6) and (7) are zero and  $G = 0$ . Hence

$$F + G - H = (x' - x)a \cos \theta - (y' - y)b + \left( \frac{a^2}{2} \cos^2 \theta + \frac{b^2}{2} \right) (z_0 - z) \quad (19)$$

gives the phase used in the computation of the resolution function.

### C. Subreflector and Quadrapod Blockage

The subreflector and its quadrapod support structure produce considerable blockage and diffraction side lobes from this blockage. This blockage is very complete in the shadowed regions and the information from the holographic maps in these regions is not usable. We attempted to use diffraction modeling to correct the regions adjacent to the blockage with some success but we found it better to increase the size of the regions which were blanked before input to the mechanical model. We found that the quadrapod structure was so complicated that accurate diffraction modeling was difficult, although in principle it should be possible.

## V. MAGNITUDE OF RADOME AND OTHER CORRECTIONS

Table II gives the approximate peak magnitude of the various corrections for the holography measurements made at

TABLE II  
PEAK MAGNITUDE OF VARIOUS CORRECTIONS USED IN THE  
HOLOGRAPHIC MAPPING OF THE HAYSTACK ANTENNA AT 12 GHz

	Resolution cm	Magnitude mm	Comments
Radome hubs	50	1	typical hub
Radome hubs	90	0.4	
Radome spars	50	0.2	increase at edge of dish
Radome spars	90	0.1	
Subreflector diffraction	90/50	0.3	outer edge of dish
Feed phase	90/50	0.3	astigmatism

12 GHz with resolutions of 50 cm and 90 cm respectively. The magnitudes are given in an equivalent surface deviation which is equal to half the phase path correction. The Cassegrain feed used for holography on the Haystack antenna is a long pyramidal horn whose phase pattern over the angle subtended by the subreflector is very smooth with only a small residual astigmatism.

## VI. EXAMPLES OF RESULTS

### A. Measurement Method

An interferometer is formed between the Haystack antenna and a small satellite TV dish located about 50 m away. The microwave receiver outputs are down-converted to an IF band and then further down-converted to baseband and one-bit sampled using a Mark III VLBI data acquisition rack [9]. The signals are correlated in real time using a direct connection from the formatter to the Mark III correlator which eliminates the tape recorder used for VLBI. Four Mark III baseband converters are used, each with 0.5 MHz bandwidth to provide two simultaneous data channels. The converters are programmed to select a pair of pseudo-noise channels separated by about 4 MHz. The 0.5 MHz bandwidth was chosen to match the pseudo-noise channels transmitted by the satellite. The complex correlations are merged with total power calibration data and antenna raster scan data to form the input to image reconstruction software. During the raster scan there are periodic returns to the main beam in order to calibrate the instrumental phases. Table III gives some of the parameters used in the mapping.

The signal-to-noise ratio (SNR) of the interferometer was sufficient to make the random noise errors discussed by Rochblatt and Rahmat-Samii [12] much smaller than the systematic errors introduced by the radome and multiple reflections.

### B. Correction Models

Fig. 3 shows the radome diffraction correction models for maps with 50 and 90 cm resolution. Both the hubs and the spars are clearly visible in the high-resolution models. The effect of the change of smearing with location on the surface is most evident in the high-resolution amplitude correction of Fig. 3(d). Note that in this figure the hubs and spars appear

TABLE III  
PARAMETERS USED IN THE HOLOGRAPHIC MAPPING  
OF THE HAYSTACK ANTENNA AT 12 GHz

nominal azimuth limits of raster scan	$\pm 1.46^\circ$ on sky
nominal separation of azimuth scans	$0.032^\circ$ in elevation
scan rate*	$0.1^\circ/\text{s}$
time to complete 91 line raster scan	2 h
nominal wavelength	2.54 cm
map grid size	$256 \times 256$
spacing between points	17.7 cm
resolution with $2.9^\circ$ diameter circular window	50 cm
resolution with $1.6^\circ$ diameter circular window	90 cm

\*For satellite at  $31^\circ$  elevation

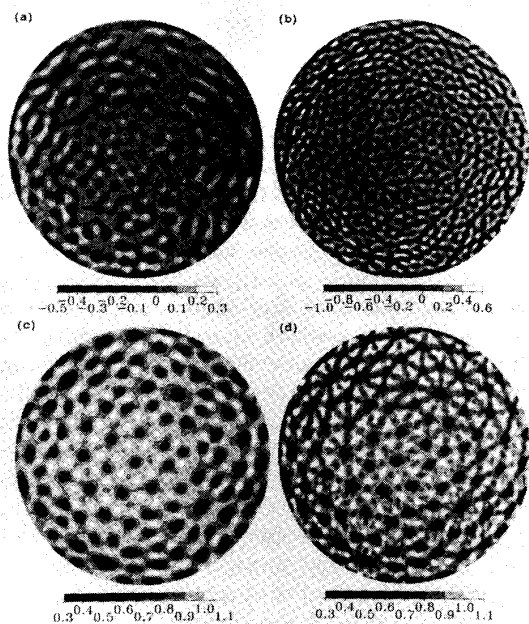


Fig. 3. Corrections for Haystack radome diffraction at 12 GHz for satellite at an azimuth of  $222^\circ$  and an elevation of  $32^\circ$ . The scale for the phase correction maps is in millimeters of equivalent surface deviation. Positive corrections (light shades) correspond to a raised surface viewed from the front of the antenna. (a) Phase correction of 90 cm resolution. (b) Phase correction for 50 cm resolution. (c) Amplitude correction for 90 cm resolution. (d) Amplitude correction for 50 cm resolution.

sharper at the top of the dish than at the bottom. The variation of smearing with  $y$  (see (14)) is the result of the change in distance from the azimuth rotation axis. As the elevation of the antenna increases from zero, the bottom of the dish becomes further from the azimuth axis than the top of the dish.

Fig. 4 shows the correction models for the subreflector diffraction appropriate for maps with 90 cm resolution. These relatively smooth corrections are only significant near the outer

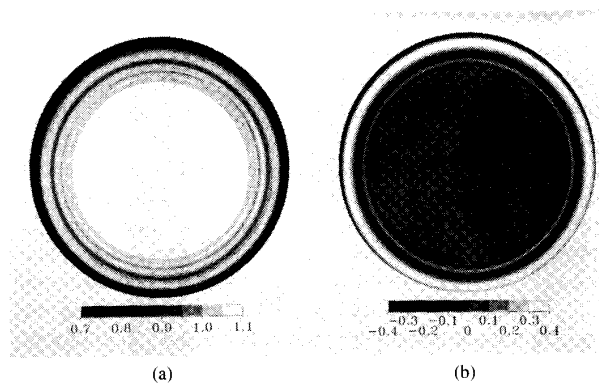


Fig. 4. Subreflector diffraction. (a) Amplitude. (b) Phase with scale in millimeters of equivalent surface deviation.

edge of the surface. The models for subreflector diffraction have been tested by making holographic maps with two different subreflector tilts and taking the difference. Since the diffraction moves with tilt, it shows up very clearly in the difference. After model correction there was little, if any, residual subreflector diffraction.

### C. Surface Maps

Fig. 5 shows the surface illumination and surface deviation maps with 50 cm resolution uncorrected and corrected for radome diffraction. Since the radome effects are less severe with 90 cm resolution (see parts (a) and (c) of Fig. 3), we show only the high-resolution maps which uncorrected are severely limited by the radome. The surface illumination is shown as one test of the radome model accuracy which can be partly judged by the lack of radome features in the corrected map. The corrected amplitude map of Fig. 5(d) clearly shows the blockage of the subreflector and its quadrupod support. Also evident are some diffraction lobes from the quadrupod. The two faint horizontal features at about 10 m radius are the result of uncorrected diffraction from quadrupod guy cables which align most closely with satellite polarization. A significant feature in the antenna surface deviation of Fig. 5(b) is the circular "splice" plate that joins the inner and outer panels of the dish. (It is difficult to adjust the splice plate so that it is perfectly aligned with the inner and the outer panels.) While the corrected phase map shown in Fig. 5(b) is relatively free of radome features, we could have "rigged" the radome into the surface. Therefore, a better test of the radome phase correction is to compare surface maps made on different satellites to expose a different radome pattern. The difference map between two satellites is shown in Fig. 6. This map was used to estimate the level of residual errors from the radome structure and panels given in Table IV. Residual errors associated with multiple reflections to the subreflector were estimated from the difference map in Fig. 7(a). These errors are given in terms of the equivalent rms surface deviation.

The map of Fig. 6(b) taken on different satellites has an rms of 0.17 mm (weighted by illumination amplitude) while the difference of two 50 cm resolution maps taken on different nights on the same satellite has an rms of 0.14

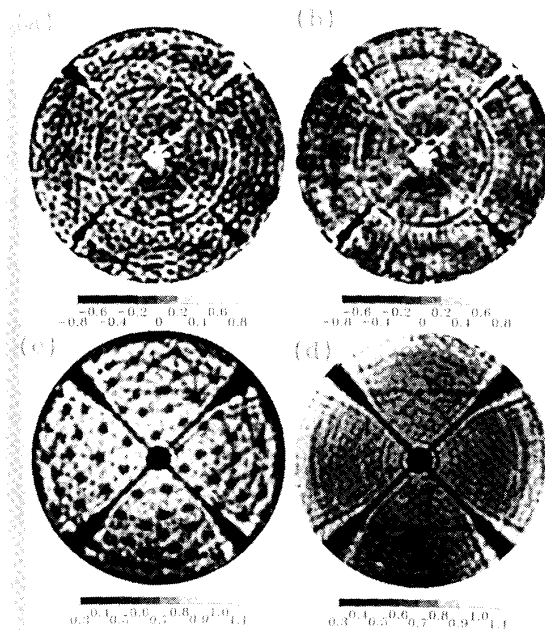


Fig. 5. Surface maps (50 cm resolution) with and without radome correction. (a) Surface deviation map without correction. (b) Corrected surface deviation. (c) Uncorrected amplitude. (d) Corrected amplitude. The scale for the phase correction maps is in millimeters of equivalent surface deviation. Both amplitude maps have a linear voltage scale with 10 dB taper correction to flatten the maps.

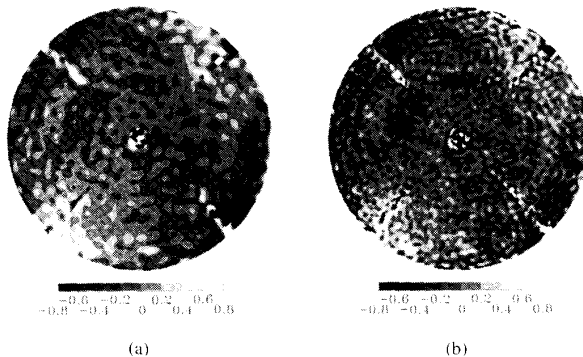


Fig. 6. Difference of surface maps between two satellites separated by 5°: (a) 90 cm resolution; (b) 50 cm resolution. Scale is in millimeters.

mm. Since the satellite moves by only a few beam widths between maps on different nights, the radome diffraction should be unchanged. However, even this small position change is sufficient to randomize the phases of the panel reflections. On the assumption that the diffraction errors repeat while the panel reflections are random, we can separate the error estimates. If the total error is the root sum square (rss) of components, then the panel reflections contribute 0.14 mm and the diffraction 0.1 mm. These numbers divided by  $\sqrt{2}$  are probably reasonable estimates of the errors in the individual

TABLE IV  
RESIDUAL ERRORS IN HOLOGRAPHY

Holography Artifact	Resolution cm	rms mm	Comments
Panel reflections	50	0.2	using single frequency
Panel reflections	50	0.1	using dual frequency
Subreflector reflections	90	0.05	from Fig. 7(a)
Residual radome diffraction	50	0.07	see text
Residual radome diffraction	90	0.04	see text
All artifacts combined	50	0.12	from Figs. 6(b) and 7(a)
All artifacts combined	90	0.10	from Figs. 6(a) and 7(a)

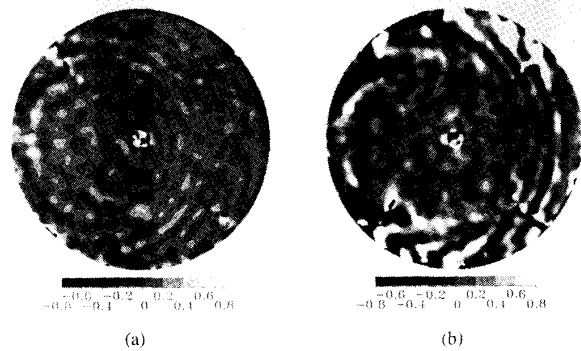


Fig. 7. Reduction of multiple reflections with spoiler: (a) with spoiler in place; (b) without spoiler—note Newton ring structure. Both of these maps are of lower quality as they were made with a single frequency.

maps and are given in Table IV for both 50 cm and 90 cm resolution. The rms surface deviation of the Haystack antenna (at the time of the map in Fig. 5(b) made in January 1992) was estimated from the 50 cm resolution holography to be 0.25 mm for Fig. 5(b) after correction for the artifacts (assuming the map is the rss of real features and artifacts). The estimate neglects components of surface roughness smaller than 50 cm which are unresolved by the holography.

VII. CONCLUSION

Diffraction effects and multiple reflections can severely limit the accuracy of antenna surface measurements made using microwave holography. The problem is especially severe if the holographic measurements have been made at a frequency much lower than the upper frequency for which the antenna will operate. The diffraction errors can be substantially reduced by modeling. Reflection spoilers and wideband holography can be used to reduce the effect of unwanted reflections. While some of the holographic errors described in this paper are unique to the Haystack antenna, the methods should be applicable to other antennas.

## ACKNOWLEDGMENT

The authors wish to thank the staff of the Haystack Observatory, especially the following: A. R. Whitney and R. J. Cappallo for setting up the correlator for real-time holography; J. A. Ball for automating the holographic raster scan; J. C. Carter for the microwave receiver and feed; M. J. Gregory for the construction of the multiple reflection spoiler; J. F. Cannon for his contributions in making the mechanical adjustments; R. P. Ingalls for the antenna thermal control and help in reviewing this paper; and J. E. Salah for his leadership and encouragement throughout the project. The authors also wish to thank M. S. Zarghamee of Simpson, Gumpertz, and Heger, Inc., and his group involved in the mechanical surface modeling.

## REFERENCES

- [1] P. F. Scott and M. Ryle, "A rapid method for measuring the figure of a radio telescope reflector," *Mon. Not. R. Astr. Soc.*, vol. 178, pp. 539-545, 1977.
- [2] J. C. Bennett, A. P. Anderson, P. A. McInnes, and A. J. T. Whitaker, "Microwave holographic metrology of large reflector antennas," *IEEE Trans. Antennas Propagat.*, vol. 24, pp. 295-303, May 1976.
- [3] H. G. Weiss, "The Haystack microwave research facility," *IEEE Spectrum*, pp. 50-69, Feb. 1965.
- [4] J. Ruze, "Antenna tolerance theory—A review," *Proc. IEEE*, vol. 54, pp. 633-640, Apr. 1966.
- [5] M. L. Meeks and J. Ruze, "Evaluation of the Haystack antenna and radome," *IEEE Trans. Antennas Propagat.*, vol. 19, pp. 723-728, Nov. 1971.
- [6] M. Born and E. Wolf, *Principles of Optics*. Oxford, England: Pergamon Press, 1987.
- [7] A. F. Kay, "Electrical design of metal space frame radomes," *IEEE Trans. Antennas Propagat.*, vol. 13, pp. 188-202, Mar. 1965.
- [8] W. V. T. Rusch, J. Appel-Hansen, C. A. Klein, and R. Mittra, "Forward scattering from square cylinders in the resonance region with application to aperture blockage," *IEEE Trans. Antennas Propagat.*, vol. 24, pp. 182-189, Mar. 1976.
- [9] T. A. Clark *et al.*, "Precision geodesy using the Mark-III very-long-baseline interferometer system," *IEEE Trans. Geosci. Remote Sensing*, vol. 23, pp. 438-449, July 1985.
- [10] W. V. T. Rusch and P. D. Potter, *Analysis of Reflector Antennas*. New York: Academic Press, 1970.
- [11] R. G. Kouyoumjian, "Asymptotic high-frequency methods," *Proc. IEEE*, vol. 53, pp. 864-876, Aug. 1965.
- [12] D. J. Rochblatt and Y. Rahmat-Samii, "Effects of measurement errors on microwave antenna holography," *IEEE Trans. Antennas Propagat.*, vol. 39, pp. 933-942, July 1991.



**Alan E. E. Rogers** (M'71) received the Ph.D. degree in electrical engineering with a thesis in radio astronomy in 1967 from MIT.

He joined the staff of the MIT Haystack Observatory in 1968 and has conducted research in radio and radar interferometry. He is a member of the research team that received the Rumford award in 1971 for the pioneering development of very long baseline interferometry (VLBI). His research includes the development of VLBI for geodesy, especially the development of the "bandwidth synthesis" method of precise group delay measurements in VLBI. He leads the VLBI group at the observatory and has developed microwave receivers and signal processing electronics and software. He worked on the development of the digitization electronics for the very long baseline array (VLBA) and is a member of the team currently working on high data rate magnetic tape recording.

Dr. Rogers is a member of the American Astronomical Society and a fellow of the American Geophysical Union.



**Richard Barvainis** was born in Binghamton, NY, in 1953. He received a B.S. in physics from the State University College of New York at Buffalo in 1976 and the M.S. and Ph.D. degrees in astronomy from the University of Massachusetts in 1978 and 1983.

In 1984 he assumed a postdoctoral research fellowship at the National Radio Astronomy Observatory in Charlottesville, VA, where he studied active galactic nuclei, polarization of stellar SiO masers, and galactic molecular clouds. With colleagues at the University of Arizona he developed a millimeter-wave polarimeter and made measurements of magnetic field directions in molecular clouds via polarization of dust emission. Since 1987 he has worked at the Haystack Observatory, first as a postdoc and then as a member of the research staff. His recent interests have centered on the nature of the continuum emission from quasars, developing models for dust emission in the infrared, and thermal free-free emission in the optical/UV region. Observational work has included measurements of carbon monoxide line emission, and submillimeter continuum emission from quasars.



**Paul Charpentier** was born in Lunenburg, MA, in 1958. In 1989 he received a B.S. in physics from the University of Lowell, Lowell, MA. He has worked at the Haystack Observatory since 1985, first as an antenna operator, becoming a staff member in 1989. His principal focus has been the pointing accuracy upgrade of the Haystack radio telescope and radio holography. Presently he is pursuing an M.S. in optics at the University of Massachusetts at Lowell.



**Brian E. Corey** was born in Akron, OH, on December 8, 1947. He received the B.A. degree in physics from Oberlin College, Oberlin, OH, in 1969 and the M.A. and Ph.D. degrees in physics from Princeton University, Princeton, NJ, in 1972 and 1978, respectively.

From 1978 to 1980 he was on the research staff of the Department of Earth and Planetary Sciences at the Massachusetts Institute of Technology. Since 1980 he has been a staff member at the Haystack Observatory, Westford, MA. His research interests include astronomical and geodetic applications of very long baseline interferometry, astronomical tests of gravitational theories, and radio astronomical instrumentation and techniques.

Dr. Corey is a member of the American Astronomical Society, the American Geophysical Union, and the American Physical Society.